# Absolute timing measurements of the Ni-like Pd and Sn soft-x-ray lasers

F. Staub,* M. Braud, and J. E. Balmer
*Institute of Applied Physics, Sidlerstrasse 5, 3012 Bern, Switzerland*

J. Nilsen
*Lawrence Livermore National Laboratory, Livermore, California 94551, USA*
(Received 1 March 2005; published 18 October 2005)

The absolute time of emission of the x-ray laser output with respect to the arrival of a 100-ps pump pulse has been measured with the aid of a calibrated timing fiducial. The results show the x-ray laser to appear up to 60 ps (80 ps) before the peak of the pump pulse in the case of the Sn (Pd) x-ray laser, which is in good agreement with simulations obtained from the LASNEX and CRETIN codes. The pulse duration was found to be ~45 ps for both the Sn and the Pd x-ray lasers.

DOI: 10.1103/PhysRevA.72.043813 PACS number(s): 42.55.Vc

## I. INTRODUCTION

Rapid progress in the development of collisionally pumped soft-x-ray lasers in recent years has led to a number of robust, saturated lasing lines using the Ne-like (e.g., Zn, Ge, Se, etc.) and Ni-like (e.g., Pd, Ag, Sn, etc.) schemes. The output properties of these lasers have been characterized in terms of the most relevant laser parameters including output energy, pulse duration, coherence, near-field and far-field energy distributions, and divergence [1–4]. Of great interest in this context is the precise knowledge of the absolute time of emission of the x-ray laser pulse with respect to the incident drive pulse, as this would permit direct comparison with simulation results and thus help to improve our understanding of the atomic-level population dynamics. Measurements for Ne-like schemes using long (~500 ps) drive pulses and the prepulse technique have revealed a marked difference in emission time for the $J=0-1$ line as compared to the $J=2-1$ lines which were found to peak 200–300 ps later in time [5,6]. In a double-100-ps pulse experiment using Ne-like Ge, Daido *et al.* reported the $J=0-1$ line to be emitted 40 ps earlier than the $J=2-1$ lines which coincided with the peak of the second pulse [7]. In the case of Ni-like lasers and multiple-150-ps-pulse pumping, $J=0-1$ lasing was reported to occur during the rising edge of the second pulse, 140 ps before the peak of the continuum emission [8,9]. Time measurements of high resolution of Ni-like Ag in the transient collisional excitation (TCE) pumping scheme were presented by Kuba *et al.* [10]. A 1.3-ps drive pulse generated a 2.4-ps x-ray laser pulse during the rising edge of the continuum emission. The absolute timing of the x-ray laser pulse with respect to the drive pulse, however, was not measured in these experiments.

In this work we describe our recent experiments aimed at measuring the absolute timing of the x-ray laser output with respect to the arrival of the drive pulse. This was achieved by implementing a calibrated timing fiducial using a frequency-quadrupled portion of the main pulse.

## II. EXPERIMENTAL SETUP

The experiments were performed using the 1054-nm Nd: glass laser system at the Institute of Applied Physics of the University of Bern (IAP-BE). The laser, having a final amplifier of 90 mm diameter, is capable of delivering up to 30 J at a pulse duration of 100 ps [full width at half maximum (FWHM)]. The output beam is focused to give a line focus of 2.5 cm length and approximately 80 $\mu$m width using a combination of a 500-mm-focal-length aplanatic doublet and a −1700-mm-focal-length cylindrical lens. Targets were 25-mm-wide slabs having a diamond-machined surface finish. A 0.5% prepulse irradiated the target 5 ns before the arrival of the main pulse. With these settings, the x-ray laser output was found to be saturated with an estimated gain-length product of 16.8 in previous work [11].

The time-resolved diagnostics setup is shown in Fig. 1. The x-ray laser emission is directed onto the 140-$\mu$m-wide slit of a Kentech 2×-magnification x-ray streak camera via a 1200-lp/mm, aberration-corrected, flat-field Hitachi grating

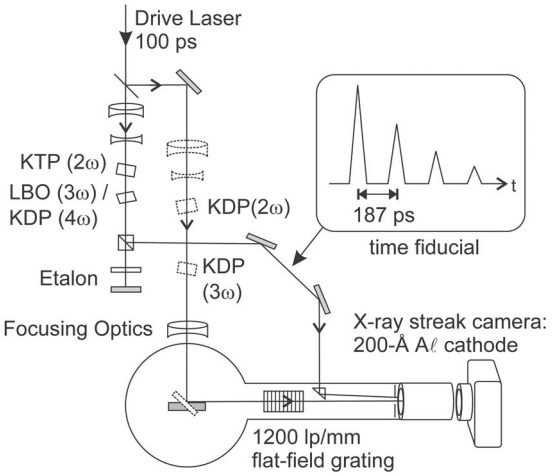


FIG. 1. Schematic of the time-resolved diagnostics with $4\omega$ timing fiducial. Dashed components are inserted for the $3\omega$ calibration measurements together with the LBO tripler instead of the KDP quadrupler used for the x-ray measurements.

*Electronic address: felix.staub@iap.unibe.ch

 

spectrograph. The streak camera is equipped with a transmission photocathode made up of a 200-Å-thick layer of aluminum deposited on a 1200-Å-thick Formvar foil. The use of the standard (more sensitive) CsI cathode was rejected here because of a delay of the photoelectrons in the order of 50 ps that was observed for the 1200-Å-thick CsI layer which might introduce an unnecessary error to the measurements.

The streaked signal is read out by an image intensifier coupled to a cooled charge-coupled-device (CCD) camera having a pixel size of 23 $\mu$m. To avoid saturation of the streak camera, a 10-$\mu$m-wide slit and several Al-on-Formvar filters were inserted at the entrance of the spectrograph [12]. The (instrumental) time resolution of the streak camera was ~15 ps.

To generate a timing fiducial pulse, a fraction of the main pulse was extracted after the last amplifier turning mirror, frequency-quadrupled in a potassium titanyl/dihydrogen phosphate (KTP/KDP) crystal pair, and relayed to the streak camera cathode. A two-mirror étalon in the reference beam having a temporal separation of the echo pulses of 187 ps was inserted to check the calibration of the sweep speed of the streak camera on each shot.

The timing fiducial was calibrated with respect to the main pulse in an auxiliary experiment. For this purpose, a KDP/KDP crystal pair was inserted in the main beam line to generate a frequency-tripled pulse along the x-ray laser beam path. In order to avoid differences in the delay of photoelectrons in the Al cathode generated by photons below ($3\omega$) and above ($4\omega$, x rays) the work function of Al (4.2 eV), the timing fiducial was driven at $3\omega$ during calibration as well, by using a LBO tripling crystal instead of the KDP quadrupler.

A 45° turning mirror positioned at the target center served to direct the $3\omega$ "main" pulse to the entrance of the flat-field spectrograph. Using the grating reflection in zeroth order and shifting the streak camera to the corresponding position, the $3\omega$ "main" and $3\omega$ fiducial pulses could be recorded on one and the same shot. In this way, the two pulses could be timed with respect to each other with an accuracy of ±7 ps. The calibration was confirmed with an optical streak camera (IMACON 600) in fundamental light at 1054 nm and was found to be within the error of the $3\omega$ calibration. It is important to note, here, that the calibration refers to the *center* of the x-ray laser target. For x rays reaching the streak camera from the far end of the gain region, the additional time of propagation (~42 ps for half the target length of 25 mm) will have to be accounted for in the analysis of the results.

## III. RESULTS

For the actual x-ray laser timing experiments, the auxiliary components were removed, the timing fiducial equipped with the $4\omega$ KDP crystal, the focusing optics put back in place, the target inserted, and the streak camera shifted back in position to record the x-ray spectrum in first order. Again, the measurements refer to the *center* of the target. Figure 2 shows the streak record (raw data) for a ~12-TW/cm$^2$ shot on a Sn target. Clearly visible are the $4\omega$ timing fiducial (top) with the echos from the étalon mirror, the Sn x-ray laser (bottom), and the continuum emission.

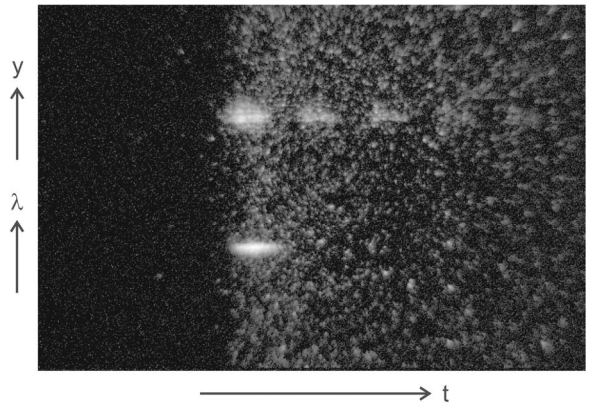


FIG. 2. Raw streak record from a 12-TW/cm$^2$ shot on a Sn target. Clearly visible are the $4\omega$ timing fiducial (top) with the echos from the étalon mirror, the Sn x-ray laser (bottom), and the continuum emission. For the x-ray laser the vertical axis corresponds to the direction of spectral dispersion ($\lambda$), while it represents the spatial coordinate of the $4\omega$ timing fiducial ($y$).

The temporal profiles obtained from the data of Fig. 2 are shown in Fig. 3 for the drive pulse, derived from the $4\omega$ timing fiducial (dashed line), the Sn x-ray laser (solid line), and the continuum emission (dotted line). We note that the first pulse of the timing fiducial seen in Fig. 2 is not simultaneous to the drive pulse shown in Fig. 3, but differs by the amount measured in the calibration experiment described in Sec. II. It is seen that the 11.9-nm lasing occurs very early during the rising edge of the main drive pulse and has a FWHM duration of 37 ps. The time by which the peak of the x-ray laser pulse precedes the peak of the drive pulse is 57 ps for this shot.

Similar results were obtained for the Pd x-ray laser at 14.7 nm, and these were modeled by means of one-dimensional (1D) computer simulations using the LASNEX and CRETIN codes. The LASNEX code [13] calculates the hydrodynamic evolution of the plasma including an expansion angle of 15° in the lateral direction to partially simulate the 2D effects. The temperatures and densities from LASNEX are used as the input to the CRETIN code [14], which calculates the gains of the laser lines including radiation trapping effects for the four strong $4f$ and $4p$-$3d$ resonance lines in

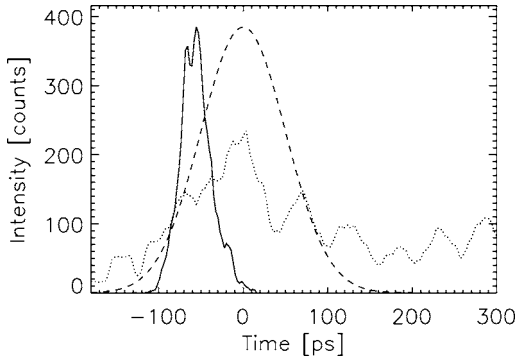


FIG. 3. Temporal profiles of the drive pulse derived from the $4\omega$ timing fiducial (dashed line), the Sn x-ray laser (solid line), and the continuum emission (dotted line) for a 12-TW/cm$^2$ shot.

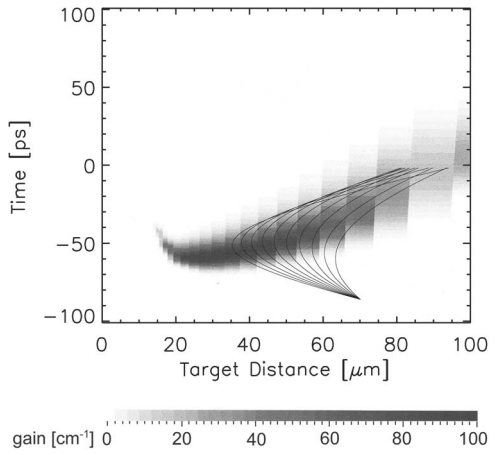


FIG. 4. Calculated temporal and spatial evolution of the gain for the Ni-like Pd line at 14.7 nm in the case of a 0.5% prepulse at 5 ns delay. Zero on the time axis corresponds to the peak of the drive pulse at the center of the target. A fan of rays obtained by ray tracing is shown to follow the gain profile due to refraction (solid curves).

Ni-like Pd. Bulk Doppler effects due to the expansion of the plasmas are also included. The Pd atomic model used by the CRETIN code includes all 107 detailed levels up to $n=4$ in Ni-like Pd. Figure 4 shows the temporal and spatial evolution of the gain for the nickel-like palladium line in the case of a 0.5% prepulse at 5 ns delay and an irradiance of 10 TW/cm$^2$. The horizontal axis gives the distance in microns from the flat target surface while the vertical axis gives the time in picoseconds with 0 ps representing the peak of the drive pulse with respect to the center of the target. Also shown is a fan of rays (solid curves) obtained by ray tracing the x-ray laser beam through the plasma column. With the rays starting from a virtual point at about $-88$ ps, they are seen to follow the gain region as a consequence of refraction in the electron density gradient, which is obtained from LASNEX calculations. The net effect is to increase the gain duration significantly. The temporal extent of the fan is 83 ps, which corresponds to the transit time along the 25-mm plasma column. The ray fan shown is chosen in order to match the divergence, the refraction angle, and the distance of the emission region from the target with previous results [4].

Figure 5 shows the temporal profiles of a typical streak record obtained at an irradiance of $\sim$9 TW/cm$^2$ on a Pd target. The figure shows the drive pulse, derived from the $4\omega$ timing fiducial (dashed line), the Pd x-ray laser (solid line), the calculated laser emission derived from ray tracing through the gain region of Fig. 4 (dash-dotted line), and the continuum emission (dotted line). The x-ray laser has a FWHM duration of 39 ps and precedes the drive pulse by 45 ps, which is in excellent coincidence with the peak of the calculated laser emission (48 ps before the drive pulse). The duration of the calculated emission is in fair agreement with the measurement. As indicated by the ray tracing in Fig. 4, the x rays do not cross the gain region at constant distance from the target (parallel to the time axis), but are refracted away from the target, following the gain plume in time and

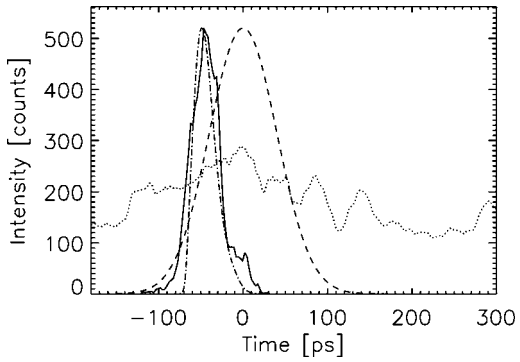


FIG. 5. Temporal profiles of the drive pulse derived from the $4\omega$ timing fiducial (dashed line), the Pd x-ray laser (solid line), the calculated laser emission (dash-dotted line), and the continuum emission (dotted line) for a 9 TW/cm$^2$ shot.

space. This leads to an increased effective gain duration, as a considerable fraction of the length of the plasma column contributes to the gain-length product. The effect of gain saturation was found to additionally lengthen the pulse duration and was taken into account for the calculation.

The peak of the continuum emission is in fair coincidence with the peak of the drive pulse, an assumption that is often made in time-resolved experiments lacking an absolute timing fiducial. However, the continuum is much broader and weaker compared to the $4\omega$ timing fiducial, making it difficult to accurately determine the time of maximum emission.

For some shots we observed strongly modulated or even double-pulse-like lasing, most of which in coincidence with similarly, but less deeply modulated drive pulses. However, each component of such double pulses showed a duration similar to proper single pulses, and all x-ray lasing occurred during the rising edge of the drive pulse.

In order to see how the irradiance of the drive pulse affects the time of emission of the x-ray laser pulse, a series of shots were taken at reduced drive irradiance. Figure 6 shows a plot of $\Delta t = t_{\text{pump}} - t_{\text{x-ray}}$ for the Sn (open squares) and Pd (diamonds) x-ray lasers, with positive values of $\Delta t$ meaning that the peak of the x-ray laser pulse is preceding the peak of the drive pulse. The emission of the Sn laser is seen to occur about 10–15 ps closer to the peak of the drive pulse as com-

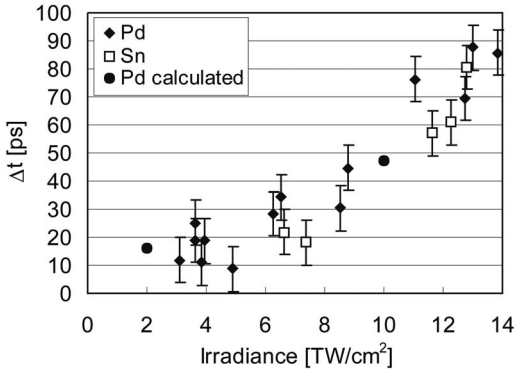


FIG. 6. Dependence of $\Delta t = t_{\text{pump}} - t_{\text{x-ray}}$ on the drive irradiance for the Sn (open squares) and Pd (diamonds) x-ray laser. Calculated points from simulations for the Pd laser are included (dots).

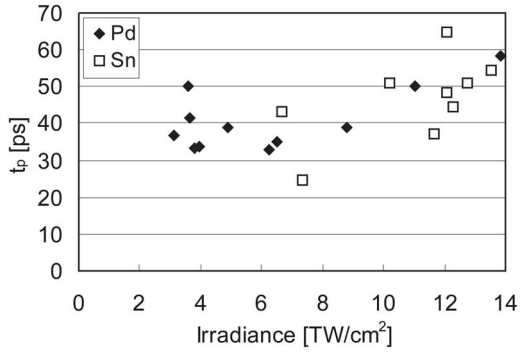


FIG. 7. Dependence of the pulse duration $t_p$ on the drive irradiance for the Sn (open squares) and Pd (diamonds) x-ray laser.

pared to the Pd laser at the same irradiance. This can be explained by the higher electron temperature needed to populate the excited states in Ni-like Sn than in Pd. Also included in Fig. 6 are two calculated points for Pd (dots), obtained from simulations with the LASNEX and CRETIN codes as discussed above, which are seen to be in good agreement with the measurements. It is clearly seen that the higher the drive irradiance, the earlier the x-ray lasing occurs. For the sake of clarity, only the most intense shots of each range of irradiance are plotted. Pulses showing weaker lasing due to nonideal plasma conditions exhibit smaller values of $\Delta t$, meaning that lasing occurs later in the rising edge of the drive pulse than for ideal shots. However, for the whole range of the measurements, x-ray lasing was seen to occur during the rising edge of the drive pulse, and only at very low irradiance does it appear close to the peak of the drive pulse.

The time of emission is determined by the rates for ionization, excitation, and deexcitation, which at the instance of optimum combination lead to maximum gain at a time depending on the above rates and their corresponding time constants. Enhanced irradiance $I$ with higher $\partial I/\partial t$ gives rise to the processes with short time constants, such as collisional excitation, in favor of the slower processes like (over)ionization. This leads to a faster rise and a higher peak value of the gain earlier in time as compared to lower irradiances, before the gain decreases due to overionization. This results in increasing x-ray laser intensity earlier in time for higher drive irradiance.

Figure 7 shows the FWHM pulse duration $t_p$ of the x-ray laser emission for Pd (diamonds) and Sn (open squares) for varying irradiance. Again, only the most intense shots of each range of irradiance are plotted. As can be seen, the dependence of $t_p$ on the irradiance is only marginal and very similar for Sn and Pd, with a slight increase of $t_p$ for increasing irradiance. The analysis of the data yielded mean values for $t_p$ of $50\pm8$ ps ($54\pm6$ ps) for Sn (Pd) at irradiances above 10 TW/cm$^2$ and $34\pm13$ ps ($38\pm5$ ps) for Sn (Pd) at irradiances below 10 TW/cm$^2$, respectively. The overall average pulse duration was $47\pm11$ ps for Sn and $41\pm8$ ps for the Pd x-ray laser, respectively.

## IV. CONCLUSIONS

Measurements of the absolute timing and the pulse durations of the Ni-like Sn and Pd x-ray lasers have been performed and compared with numerical simulations of the LASNEX and CRETIN codes. The use of a calibrated timing fiducial allowed precise measurements of the time of the x-ray laser emission with respect to the drive pulse, and no assumptions about the timing of the continuum emission enter the measurements. However, the continuum was generally found to be in good coincidence with the drive pulse. The dependence of the emission time on irradiance was measured and found to be in good agreement with the numerical simulations. A qualitative discussion of population dynamics provides a possible interpretation of the observed behavior of the time of emission on varying irradiance. The effective gain duration was found to be increased by refraction and saturation.

## ACKNOWLEDGMENTS

The authors would like to acknowledge the technical assistance of B. Locher and W. Lüscher for target preparation. This work was supported in part by the Swiss National Science Foundation. The work of J.N. was performed under the auspices of the U.S. Department of Energy by the University of California Lawrence Livermore National Laboratory under Contract No. W-7405-Eng-48.

[1] J. Zhang *et al.*, Phys. Rev. Lett. **78**, 3856 (1997).
[2] J. Nilsen *et al.*, Phys. Rev. A **56**, 3161 (1997).
[3] J. Y. Lin *et al.*, Opt. Commun. **158**, 55 (1998).
[4] C. Siegel, M. Braud, J. E. Balmer, and J. Nilsen, Opt. Commun. **210**, 305 (2002).
[5] J. Nilsen, J. C. Moreno, B. J. MacGowan, and J. A. Koch, Appl. Phys. B: Photophys. Laser Chem. **57**, 309 (1993).
[6] P. Lu, Y. Li, and E. E. Fill, Phys. Rev. A **54**, 5193 (1996).
[7] H. Daido *et al.*, Opt. Lett. **20**, 61 (1995).
[8] J. Nilsen and J. C. Moreno, Opt. Lett. **20**, 1386 (1995).
[9] H. Daido *et al.*, Phys. Rev. Lett. **75**, 1074 (1995).
[10] J. Kuba *et al.*, J. Phys. IV **11**, PR2–43 (2001).
[11] J. E. Balmer, M. Braud, and F. Loewenthal, J. Phys. IV **11**, PR2–137 (2001).
[12] M. Braud, C. Siegel, J. E. Balmer, and J. Nilsen, in *X-Ray Lasers 2002*, edited by J. J. Rocca, J. Dunn, and S. Suckewer, AIP Conf. Proc. No. 641 (AIP, Melville, NY, 2002), p. 154.
[13] G. B. Zimmerman *et al.*, Comments Plasma Phys. Controlled Fusion **2**, 51 (1975).
[14] H. A. Scott, J. Quant. Spectrosc. Radiat. Transf. **71**, 689 (2001).